The structure of liquid $AlCl_3$ and structural modification in $AlCl_3$-MCl (M=Li, Na) molten salt mixtures

1994 J. Phys.: Condens. Matter 6 10193

(http://iopscience.iop.org/0953-8984/6/47/004)

J. Phys.: Condens. Matter 6 (1994) 10193–10220. Printed in the UK

The structure of liquid $AlCl_3$ and structural modification in $AlCl_3$–MCl (M = Li, Na) molten salt mixtures

Y S Badyal, D A Allen† and R A Howe
Physics and Astronomy Department, University of Leicester, Leicester LE1 7RH, UK

Received 12 August 1994, in final form 12 September 1994

Abstract. The scattering from pure liquid $AlCl_3$ and $AlCl_3$–MCl (M = Li, Na) binary molten salt mixtures has been measured by time-of-flight neutron diffraction. Reverse Monte Carlo simulation of the $AlCl_3$ data, whilst confirming a regular tetrahedral local geometry for the Al^{3+} ion, challenges the accepted view of the structure as consisting (predominantly) of discrete Al_2Cl_6 dimers. The data for the mixtures suggest that the connectivity in the structure of pure $AlCl_3$, formed by Al–Cl–Al bridges, is proportionately reduced upon the addition of alkali halide as isolated $AlCl_4^-$ units are created. In addition, a gradual shift in the position of the first sharp diffraction peak to higher Q is observed, implying a systematic reduction in the length scale of intermediate-range order. The findings for the mixtures are generally consistent with those from previous structural studies using x-ray diffraction and also with Raman and electrochemical measurements.

1. Introduction

In contrast to the large number of structural studies undertaken on pure molten salts, comparatively little work has been done on molten salt mixtures. This is despite the fact that molten salt mixtures often exhibit attractive properties such as low-temperature eutectics of possible relevance to energy storage and other commercial applications. The relatively low-melting acidic (i.e. those containing more than 50% $AlCl_3$) $AlCl_3$–MCl (M = Li, Na) mixtures, which are the subject of the current study, are a particularly good case in point. These melts are also of interest because they are part of a class of complexing binary systems whose thermodynamic and physical properties display strong compositional dependences that are not completely understood. In this paper, we describe the results of a neutron diffraction study undertaken as part of an ongoing structural investigation of binary molten salt mixtures [1–3].

There is considerable evidence for the existence of a series of complex ions, $AlCl_4^-$, $Al_2Cl_7^-$ and $Al_3Cl_{10}^-$, in alkali chloroaluminate melts for acidic compositions. The presence of such structural units was first reported in studies of $AlCl_3$–NaCl melts by Raman-spectroscopic analysis [4] and thermodynamic measurements [5]. The proportion of $Al_2Cl_7^-$ ions was found to increase with $AlCl_3$ concentration and at compositions close to the pure salt endpoint the presence of an additional species, most likely $Al_3Cl_{10}^-$, was indicated. The proportion of isolated $AlCl_4^-$ tetrahedra was also shown to increase with temperature at all compositions. More recently, these trends have been confirmed for $AlCl_3$–NaCl and $AlCl_3$–KCl molten salt mixtures by x-ray [6] and neutron diffraction [7] studies, respectively. All

† Present address: School of Physics and Space Research, University of Birmingham, Edgbaston, Birmingham B15 2PT, UK.

0953-8984/94/4710193+28$19.50

the complex ion species are essentially polymeric—being based on the same fundamental unit of $AlCl_4^-$ tetrahedra sharing corners. However, the precise structures are not well established and there is some disagreement as to whether the higher-order species ($Al_2Cl_7^-$ etc) have a linear or, as suggested by *ab initio* molecular-orbital (MO) calculations [8], which take into account the effects of bond polarization, a bent Al–Cl–Al bridge. Blander *et al* [7] achieved optimum fits to structure factor data for acidic AlX_3–KX (X = Cl, Br) melts using a bent-bridge angle of approximately 110° for $Al_2X_7^-$ which was consistent with MO calculations and the x-ray diffraction analysis of crystalline KAl_2Br_7 [9].

In contrast to the $AlCl_3$-rich melts, the equimolar compositions are regarded as relatively simple systems consisting mainly of $AlCl_4^-$ tetrahedra and alkali cations. The EMF measurements of Boxall *et al* [5] indicate this is the case for the $AlCl_3$–NaCl system and also suggest a high degree of charge ordering between complex anions and alkali counter-ions, a model which appears to be confirmed by analysis of x-ray-diffraction data for equimolar $AlCl_3$ + LiCl [10] and $AlCl_3$ + NaCl [11] molten salt mixtures.

In our earlier studies [2, 3] of divalent metal chloride–alkali chloride melts, we reported similar charge-ordered structures for systems such as $NiCl_2$–KCl near the critical $\frac{2}{3}$ alkali halide concentration. The formation of a charge-ordered structure in mixtures involving 2:1 molten salts appears to be dependent on the type of alkali cation—large ions such as K^+ promote structural modification whereas small ions such as Li^+ give rise to admixtures of the pure salt structures—and also seems to be associated with enhanced intermediate-range order (IRO). In order to explore the effects of reducing the size of metal cation and hence greatly increasing its polarizing power, we have extended our studies to the trivalent metal chloride–alkali chloride molten salt mixtures which are the subject of the current paper.

The secondary aim of our investigation was to gain further insight into the structure of pure liquid aluminium chloride, not only by measurement of the total structure factor for the pure salt but also from the structural modification observed in the mixtures. The established model of molten $AlCl_3$ is that of a fluid of Al_2Cl_6 dimers each formed by edge sharing of two somewhat distorted $AlCl_4^-$ tetrahedra. The anomalously large volume increase upon melting from an octahedral coordination in the crystal ([12] and references therein) and the results of an early (1951) x-ray diffraction study of the liquid [13] are often cited in support of this rather idealized model. However, $AlCl_3$ and $ZnCl_2$, which is believed to have a very different 'network liquid' ([1] and references therein) structure made up of corner-linked $ZnCl_4^{2-}$ tetrahedra, share some intriguing similarities in their physical properties, e.g. a low melting point and very low conductivity in the melt. In the light of this observation, we have undertaken a detailed analysis, including reverse Monte Carlo (RMC) modelling, of our neutron diffraction data for liquid $AlCl_3$. RMC has also provided partial structure factor (PSF) information, which has facilitated analysis of the data for the mixtures.

2. Theory

The aim of a neutron diffraction experiment is to measure the total structure factor, $F(Q)$. This is defined for a two-component system with atoms of types a and b by the following relation:

$$F(Q) = c_a^2 b_a^2 (S_{aa}(Q) - 1) + c_b^2 b_b^2 (S_{bb}(Q) - 1) + 2c_a c_b b_a b_b (S_{ab}(Q) - 1) \qquad (1)$$

where c_α is the concentration and b_α is the coherent scattering length of species α. The $S_{\alpha\beta}(Q)$ terms are the PSFs according to the definition of Faber and Ziman [14]. $S_{\alpha\beta}(Q)$ is

related to the pair distribution function, $g_{\alpha\beta}(r)$, by Fourier transformation as shown below:

$$g_{\alpha\beta}(r) = 1 + \frac{1}{2\pi^2\rho_0}\int_0^\infty Q^2(S_{\alpha\beta}(Q) - 1)\frac{\sin(Qr)}{Qr}\,\mathrm{d}Q \tag{2}$$

where ρ_0 is the number density. Substitution of (2) into (1) leads to an expression for the Fourier transform (FT) of $F(Q)$ known as the total pair distribution function or $G(r)$, which can be written as

$$G(r) = 1 + c_a^2 b_a^2(g_{aa}(r) - 1) + c_b^2 b_b^2(g_{bb}(r) - 1) + 2c_a c_b b_a b_b(g_{ab}(r) - 1). \tag{3}$$

Not surprisingly, $G(r)$ is a linear sum of the various partial structures, weighted for concentration and scattering, just as in the original $F(Q)$ function. The precise form of the equations shown is only valid for pure molten salts containing two types of atom, such as liquid $AlCl_3$. In the case of the molten salt mixtures studied, there are three types of atom so the above equations have to be generalized to incorporate six partial structures.

3. Experimental details

The mixtures were prepared using pure ($\geqslant$ 99.99%) anhydrous single salts heated under vacuum to minimize their moisture content. However, vacuum drying could not be used for $AlCl_3$ because of its high vapour pressure. Instead, a method of sublimation drying was employed with the salt being heated gradually (over a period of about 3 d) to approximately 150 °C whilst being continually evacuated by a diffusion pump. The sublimed salt vapour was collected in a condensation trap ($\sim$ −5 °C) leaving most of the water vapour to continue to the pump. Microanalysis gave an *upper* limit for the concentration of water in the sublimed $AlCl_3$ of $\sim$ 0.5% by weight. Mixtures of the desired composition were obtained by weighing out the appropriate masses of the dried salts. The general sample preparation procedure is detailed by Allen *et al* [1]. The LiCl used in mixtures with $AlCl_3$ was isotopically enriched ($\geqslant$ 99.99%) in ^{7}Li to avoid the very large absorption cross-section for neutrons of the ^{6}Li isotope.

The data were collected in two separate time-of-flight (TOF) neutron diffraction experiments using the SANDALS instrument at Rutherford ISIS. In the first, the scattering was measured for samples of 0 (200 °C), 30 (300 °C), 45 (300 °C), 70 (740 °C) and 100% (820 °C) NaCl with $AlCl_3$. In the second experiment, measurements were made for samples of 25 (280 °C), 50 (280 °C), 70 (625 °C) and 100% (640 °C) LiCl with $AlCl_3$. Multiple scans were performed for each sample to check whether structural changes in sample or container, from incomplete mixing or chemical attack, occurred during data collection. Only scans that agreed to within statistical error were integrated. In both experiments, data were collected for the empty container (at low and high temperatures close to the pure-salt melting points), furnace backgrounds and a vanadium calibration.

The raw data were analysed using the Rutherford ATLAS package [15]. The procedure followed was much the same as described by Allen *et al* [1] for analysing LAD data except in the use of corrections for furnace as well as container scattering. Reliable furnace corrections were essential because of the very large furnace background on SANDALS. Even with appropriate corrections (details of the precise parameters and how they were chosen are given elsewhere [16]) there was marked disagreement between the vanadium calibrated scattering from different detector groups. This is believed to be due to sample-dependent background scattering, which, fortunately, appears to be mostly in the form of

monotonic Q-space slopes evident as spurious features at low r in real space. The problem was minimized using the program SUBSELF [17], which effectively corrected the scattering by fitting a theoretical low-r base level (based on sample composition) to the FT and then back transforming. The resulting excellent agreement between detector groups made inelasticity corrections redundant, and also meant that data could be merged over a wide Q range, thus generating composite $F(Q)$ functions with improved statistics. Because of the lack of isothermal compressibility data, the experimentally inaccessible low-Q portion of the data was simply extrapolated. Fortunately, because of the Q^2 dependence of the FT this makes little difference to the real-space picture.

The $G(r)$ functions were obtained by Fourier transformation of $F(Q)$ data smoothed at high Q. No window function was employed. In each case, comparison of the $G(r)$ derived from the smoothed and unsmoothed $F(Q)$ data confirmed that mainly Fourier ripple was removed with marginal effect on real peaks (see figures 1 and 2).

The data-analysis parameters for the pure salts are given in table 1. The density data used for the $AlCl_3$-rich mixtures with LiCl and NaCl were taken from [20] and [21], respectively. In the absence of published measurements, the number densities for the 70% alkali halide compositions were linearly interpolated from temperature-extrapolated values for the equimolar and pure alkali halide melts.

Table 1. Data-analysis parameters including the Faber-Ziman (FZ) coefficients for the pure salts. The temperatures corresponding to the density figures are in brackets. The symbol M denotes the relevant metal species in the case of each pure salt. The scattering cross-sections are from Sears [18].

Pure salt	Number density ρ_0 (Å^{-3})	FZ coefficients M–M	M–Cl	Cl–Cl
$AlCl_3$	0.023 (200 °C)[a]	0.007	0.124	0.516
NaCl	0.032 (820 °C)	0.031	0.171	0.229
LiCl	0.042 (640 °C)	0.009	−0.091	〃
^{7}LiCl	—	0.012	−0.104	〃

	σ_c (barns)	σ_s (barns)	σ_a (barns) at (1.8 Å)
Al	1.49	1.5	0.23
Na	1.61	3.28	0.53
Li	0.45	1.36	70.5
^{7}Li	0.62	1.40	0.045
Cl	11.52	16.8	33.5

[a] From King and Seegmiller [19].

4. Discussion

4.1. The structure of pure liquid $AlCl_3$

The local structure of the Al^{3+} ion appears to be well defined with a regular, fourfold-coordinated tetrahedral geometry. The $F(Q)$ and corresponding $G(r)$ functions for liquid $AlCl_3$ are shown in figures 1 and 2, respectively. There is clearly a deep first minimum after the well resolved Al–Cl principal peak in real space, implying little movement of anions into and out of the first shell. The mean anion coordination number for this peak is

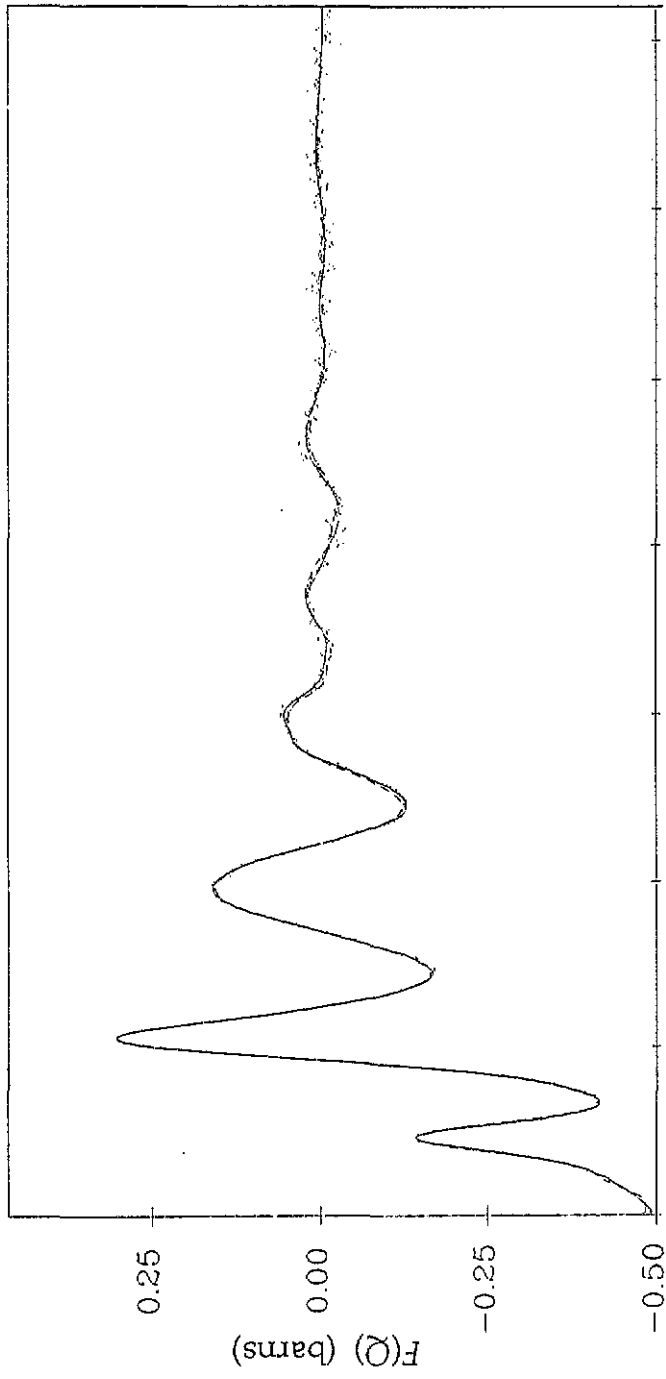

Figure 1. The total structure factor data (dotted curve) for pure liquid $AlCl_3$ compared with the function obtained by smoothing at high Q (solid) and the fit obtained using the maximum-entropy method (dashed). Note that although only a limited data range is shown in this and other figures (for clarity), the Q_{max} actually used in Fourier transformation was typically 20–24 $Å^{-1}$.

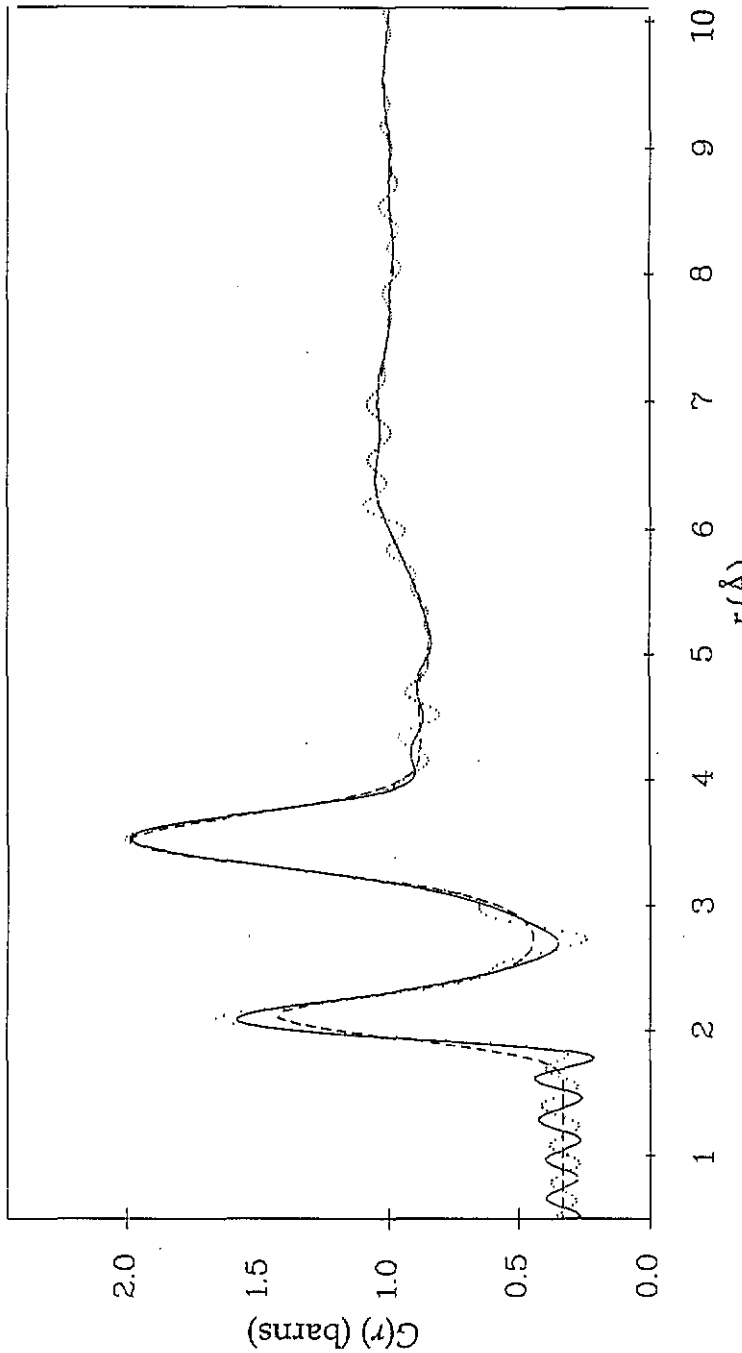

Figure 2. The total pair distribution functions for pure liquid $AlCl_3$ corresponding to the functions in figure 1. The $G(r)$ obtained from a smoothed $F(Q)$ (solid curve) is clearly less affected by spurious ripple than the transform of the original data (dotted). The maximum-entropy solution (dashed) has a noticeably broader first peak but this is often the case with this method; the agreement with the smoothed $F(Q)$ transform is very good at higher r.

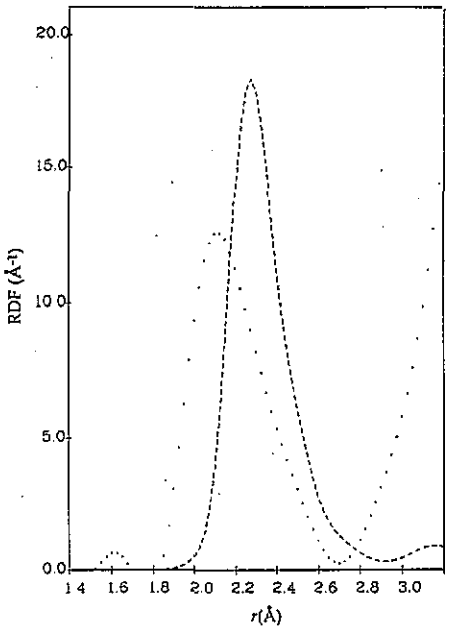

Figure 3. A comparison of RDFs, defined as $4\pi\rho_0 r^2 g(r)$, for $g^{AlCl_3}_{Al-Cl}(r)$ (dotted curve) and $g^{ZnCl_2}_{Zn-Cl}(r)$ [22] (dashed curve). The RDF for the Al–Cl function has been determined directly from our $G(r)$ data.

$\sim 4.0 \pm 0.2$ (the deep first minimum means this is a fairly reliable estimate). The r_{--}/r_{+-} ratio in $G(r)$ of ~ 1.66 is also close to that of a regular tetrahedron. However, comparison of the radial distribution functions (RDFs) for $g^{AlCl_3}_{Al-Cl}(r)$ and $g^{ZnCl_2}_{Zn-Cl}(r)$ (the superscript refers to the pure salt), as in figure 3, shows that although the principal peak in $AlCl_3$ is at lower r, it is shorter and broader with an FWHM of $\sim 0.42 \pm 0.05$ compared with $\sim 0.27 \pm 0.02$ Å for $ZnCl_2$. The reason for this is apparent from the Al_2Cl_6 molecular structure shown in figure 4 and the corresponding structural parameters in table 2. The Al–Cl principal peak is actually a combination of two overlapping peaks due to shorter, terminal, $Al–Cl^T$ and longer, bridging, $Al–Cl^B$ bonds.

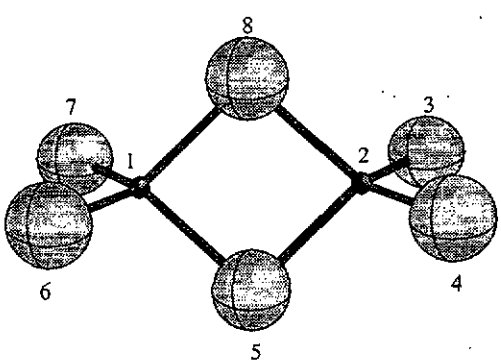

Figure 4. The Al_2Cl_6 molecular structure of liquid $AlCl_3$ as suggested by Harris *et al* [13] from x-ray diffraction measurement. The diagram has been drawn according to the parameters given in table 2, with the large Cl and the smaller Al atoms shown at $\frac{1}{3}$ scale. The dimeric molecule consists of two edge-sharing tetrahedra distorted in the Al–Al direction such that the angles formed by atoms 8–1–5 and 8–2–5 are reduced from 109.5 to approximately 90°.

Table 2. Parameters for the Al_2Cl_6 molecular structure. Cl^B and Cl^T denote the bridging and terminal chlorine atoms, respectively. The bond angles have been defined by specifying a triplet of atoms—the required angle is formed by the central atom with respect to the other two.

Al_2Cl_6 state	Bond lengths (Å)					Bond angles (°)	
	Al–Cl^B	Al–Cl^T	Al–Al	Cl^B–Cl^B	Cl^T–Cl^T	Cl^B–Al–Cl^B	Cl^T–Al–Cl^T
Vapour[a]	2.25	2.07	3.21	3.16	3.64	91.0	123.4
Quasicrystal[b]	2.29	2.08	3.26	3.21	3.64	89.1	121.8

[a] From the electron diffraction measurements of Palmer and Elliott [23].
[b] From quantum-chemical calculations [24].

However, some details of the total pair distribution function appear to be inconsistent with the established view of the structure as consisting, predominantly, of such discrete Al_2Cl_6 dimers. In this regard, it should be noted that the only previous structural study, by Harris *et al* [13] using x-ray diffraction, is fundamentally flawed. The radial distribution curve presented in this earlier study is clearly affected by large FT truncation errors—the first minimum after the Al–Cl principal peak dips well below zero, indicating a sizeable FT ripple amplitude. This error means the shape and position of the peaks must be deemed inaccurate and even puts into doubt the existence of those at high r. The absence in our neutron data of peaks corresponding to those at $r \sim 5.6$ and $r > 7.5$ Å (see figure 2), as claimed by Harris *et al*, appears to confirm the systematic errors in the earlier study. Unfortunately, Harris *et al* used their dubious values of peak position to deduce the structural parameters of the *assumed* Al_2Cl_6 dimer and obtained good agreement with the results of an electron diffraction study of the vapour phase [23] (for which there is strong evidence for the existence of dimers) thus 'confirming' their initial assumption. However, duplicating the approach of Harris *et al* and using our peaks at $r \sim 6.3$ and 7.0 Å (instead of 5.6 and 6.5 Å), whose positions were verified using the maximum-entropy method (see [1] and references therein), for the interatomic distances 4–6 and 3–6 respectively in figure 4, leads to dimers with a structure even more distorted in the Al–Al direction. The shape of the Al–Cl peak on the high-r side is not consistent with Al–Cl^B bond lengths significantly greater than those in table 2, which implies the additional distortion would involve a reduced distance between the two bridging Cl atoms. This would further intensify the 'overlap' problem of these atoms and makes such a structure appear unlikely. An alternative model involving corner sharing, in place of edge sharing, of tetrahedral units would seem more probable. The peaks at $r \sim 6.3$ and 7.0 Å agree quite closely with the two Cl–Cl distances of 6.13 and 7.0 Å obtained in a modelling study of $AlCl_3$–*n*–BPC mixtures [25] at a composition known to consist primarily of corner-sharing $Al_2Cl_7^-$ units. In addition, simple weighted averaging of the Al–Cl^T and Al–Cl^B bond lengths in table 2 provides a better match to our Al–Cl peak position of ~ 2.11 Å if polymeric corner-sharing tetrahedral units are assumed. For example, an estimate of ~ 2.13 Å is obtained for $Al_3Cl_{10}^-$ units compared with ~ 2.18 Å for discrete dimers.

Our observations call for a critical reassessment of some of the arguments usually made in support of the established model.

(i) *Electron diffraction studies of the vapour [23].* As pointed out above, the only direct structural study [13] suggesting a strong similarity between the liquid and vapour phases is seriously flawed. The vapour phase inevitably favours bound molecular states, but the liquid environment, and hence structure, may be very different. In this context, it is interesting to note that the electron diffraction data [23] also indicate a trend of increasing deformation, and hence decreasing stability, for the halide series Al_2X_6, X = I → Br → Cl, in the

vapour phase. This implies that, of the three trihalides, $AlCl_3$ is *least* likely to have a dimer structure in the liquid.

(ii) *Raman scattering experiments.* These only provide indirect evidence on structure and the usual approach to interpretation, that of iteratively refining a self-consistent force model, often depends on arbitrary initial assignments of experimentally identified modes. Even a study [24] that uses *ab initio* MO calculations to show an apparently excellent agreement between model and experiment is based on the assumption of gas-phase dimers—alternative models that could fit the data equally well, or better, do not appear to have been considered.

(iii) *The large increase in specific volume (~ 88%) and entropy upon melting of $AlCl_3$, more than twice that observed for $AlBr_3$.* This is certainly evidence of a unique structural transition but not necessarily of dimers in the liquid. The volume increase is usually explained entirely in terms of the dramatic change in coordination of the Al^{3+} ion from octahedral in the crystal [12] to tetrahedral in the melt [13]. In the case of $AlBr_3$, the Al^{3+} ion starts off with a tetrahedral coordination in a crystal molecular lattice of Al_2Br_6 dimers, which appear to be retained in the melt ([26] and references therein). Clearly, other fourfold-coordinated structures, such as the corner-sharing tetrahedral units suggested earlier, would be as consistent with this explanation as Al_2Cl_6 dimers. A further weakness in the conventional explanation is to assume the difference in crystal structure of the two salts accounts entirely for the melting behaviour. Comparison of the packing fractions for liquid $AlCl_3$ (~ 40%) and $AlBr_3$ (~ 50%) reveals the substantially greater void volume in the former, which, in the opinion of the authors, is difficult to reconcile with the notion of a similar dimer structure in both melts.

It is clear from the above, that while the evidence is strong for a dramatic change in structure from the crystal state on melting, it is very weak for specifically a dimer structure in the melt. Indeed, our development of the historical arguments leads us to favour alternative structures.

Because the use of specific features of $G(r)$ to make inferences about structure can be misleading, we have attempted to model our data. Details of the chosen method, RMC, are available elsewhere [16, 27] so we shall only give an outline of the method and its application. The RMC algorithm is a variant of the standard Metropolis Monte Carlo (MMC) algorithm—the distinction being that RMC minimizes the χ^2 fit directly to the diffraction data whereas MMC minimizes the total potential energy. A random initial configuration containing $N = 2400$ atoms satisfying the necessary closest-approach and density constraints was always used. The size of the simulation cube allowed the model $G(r)$ to be calculated up to $r \sim 23.6$ Å. An initial fit was attempted to $G(r)$ data, which allowed the closest-approach distances to be fine tuned, before restarting from a random configuration and fitting directly to the structure factor. As the model neared equilibrium (χ^2 fluctuating about a minimum), automatic renormalization of the data, to improve the fit with the model $F(Q)$, was allowed as a refinement. The renormalization factor never exceeded ±5%. Statistically independent configurations, each separated by at least $2N$ accepted moves, were collected for averaging of their properties once the model had clearly reached equilibrium.

The initial results of RMC modelling (henceforth known as model I), whilst confirming an almost regular tetrahedral local geometry for the Al^{3+} ion, further challenge the accepted view of the wider structure. The model I fit to the $F(Q)$ data is shown in figure 5, along with the weighted contributions of the RMC partials to the total scattering. The corresponding comparison in real space is shown in figure 6. The bond-angle distributions (averaged over five independent configurations) relevant to local structure are shown in figure 7. The prominent peaks at ~ 107° in the Cl–Al–Cl function, at ~ 60° in the Cl–Cl–Cl and at ~ 37° in Cl–Cl–Al agree closely with the values of 109.5, 60 and 35.25°,

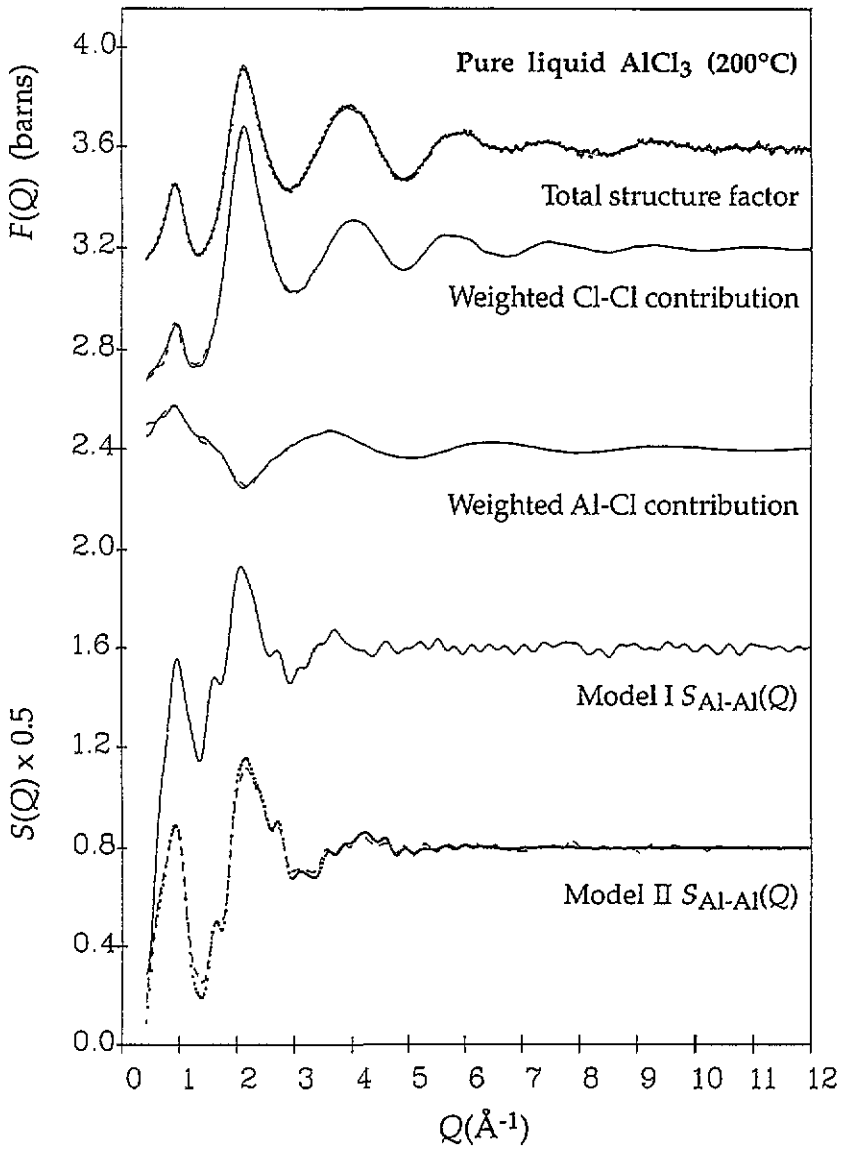

Figure 5. Total structure factor data for pure liquid $AlCl_3$ (topmost curve, dotted) compared with the RMC model fits: model I, solid curve; model II, dashed curve. The fits to the structure factor data for the two models are nearly indistinguishable and the corresponding RMC Cl–Cl and Al–Cl partial structures (shown weighted by their respective FZ coefficients) are also little different. The RMC $S_{Al-Al}(Q)$ functions are shown scaled by 0.5 for display purposes. The artificial $S_{Al-Al}(Q)$ data set used as an additional constraint for model II is shown as a dotted line, and compared against the fit, in the bottom set of curves.

respectively, of a regular tetrahedron. The coordination-number distribution (figure 8) indicates strong physical constraints against anion coordinations greater than four, with the average being ~ 3.6. The tendency of the RMC to produce a solution with maximum configurational entropy means that observed anion coordinations of less than four are not

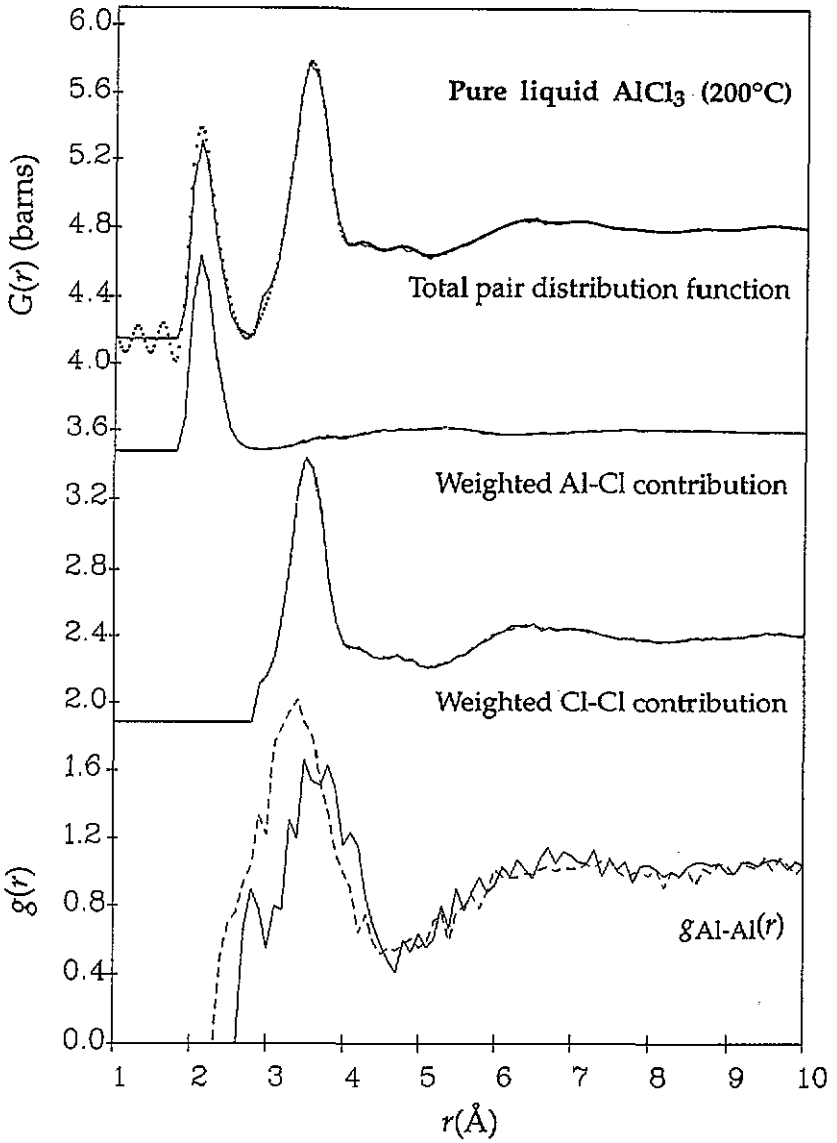

Figure 6. The total pair distribution function for pure liquid $AlCl_3$ (topmost curve, dotted) compared with the RMC model fits: model I, solid curve; model II, dashed curve. The difference between the two models is in the position of the principal peak in the $g_{Al-Al}(r)$ partial (bottom) although the Al–Cl and Cl–Cl partial structures (shown weighted by their FZ coefficients), and hence the fits to the total scattering, are almost indistinguishable.

necessarily features of the 'correct' solution—the structure may simply be insufficiently ordered. Given this characteristic, it is perhaps not surprising that the RMC structure contains few *discrete* molecules resembling Al_2Cl_6 dimers. Bond-network analysis (see table 3) reveals a large number of connected units but the majority ($\sim$ 75%) are branched chains and of the remainder—complex units containing loops and rings—only a few ($\sim$ 5%) appear to resemble Al_2Cl_6 dimers. However, this analysis also indicates few instances of

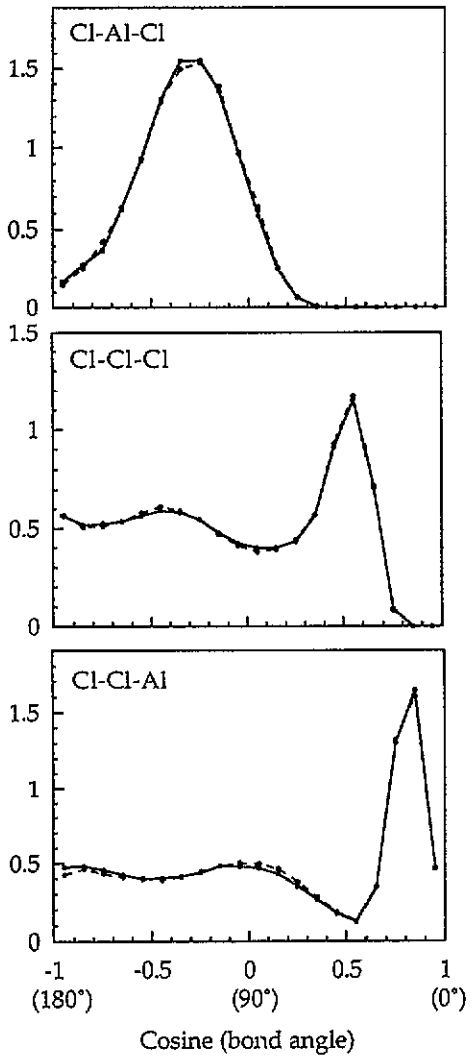

Figure 7. Bond-angle distributions relevant to local structure for model I (solid curves) and model II (dashed curves).

the essential edge-sharing feature of the dimer. This was confirmed by visual inspection of thin 'slices' through the model, thus proving that a 3D structure quantitatively consistent with the data and known physical constraints can include almost no units corresponding to dimers. The 'slice' of the model I RMC configuration shown in figure 9 illustrates the predominance of long, branched, mainly corner-linked chains of tetrahedral units with edge sharing occurring mostly within units larger than dimers.

The model I RMC structure resembles the picture of polymeric, corner-linked tetrahedra suggested earlier from semi-quantitative analysis of the $G(r)$ data. The principal peak in the model I $g^{\mathrm{RMC}}_{\mathrm{Al-Al}}(r)$ partial (the superscript denotes an RMC partial, which, in this case, has been obtained by fitting to a single data set) is centred at $r \sim 3.7$ Å, implying a mean Al–Al separation significantly greater than quoted for the vapour and quasicrystal dimer structures (see table 2). The bond-angle distributions shown in figure 10 are also consistent with predominantly corner-linked tetrahedral units. The broad peaks at $\sim 120°$ in the Al–Cl–Al function and at $\sim 25°$ in Al–Al–Cl, both indicating a bent bridge, are clearly inconsistent

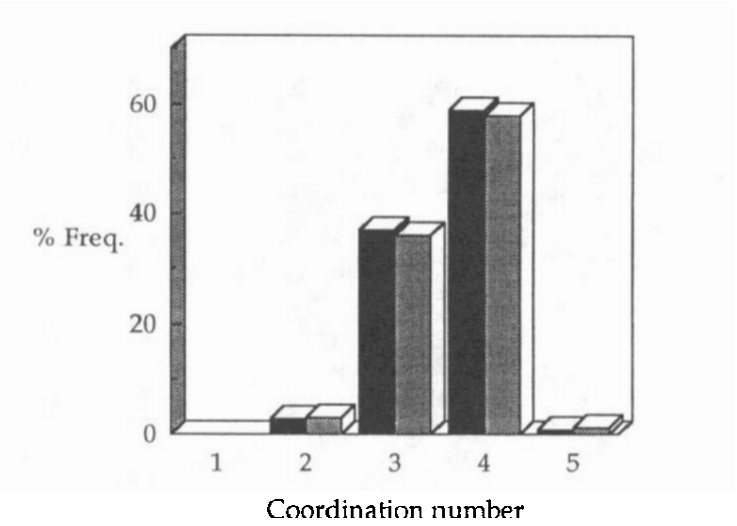

Figure 8. The coordination-number distribution of Cl anions around Al (R_{max} of 2.8 Å) for model I (black histogram) and model II (grey). The most common coordination is fourfold and the physical constraints against coordinations greater than this are apparent from the small proportion of fivefold-coordinated species.

Table 3. A comparison of the results of bond-network analysis (averaged over several configurations) for RMC models I and II. The complex units of 6–10 atoms size are the only ones that can be said to resemble discrete dimers. A small number (~ 20) of branched chains of five atoms size, corresponding to isolated $AlCl_4^-$ tetrahedra, are also apparent in both models.

	Branched chains	Complex units (with loops and rings)	
RMC model	(≥ 3 atoms size)	all sizes	6–10 atoms size
I	85	28	5
II	48	42	5

with the corresponding angles of ~ 90° and ~ 45° characteristic of the dimer. Naturally, the RMC angles are geometrically consistent with the position of the principal peak in $g^{RMC}_{Al-Al}(r)$.

Although only a single $F(Q)$ data set was available, the RMC method can apparently (through the use of physical constraints) extract a great deal of information about the structure of liquid $AlCl_3$. The most striking sign of this is the remarkably structured $g^{RMC}_{Al-Al}(r)$ partial. RMC might be expected to generate an almost unstructured Al–Al partial because of the low FZ weighting, i.e. there is little *direct* information about this partial in $F(Q)$, which implies the Al–Al structure is being 'deduced' using the more directly accessible Al–Cl and Cl–Cl partial structures. Furthermore, the mean bridging angle of ~ 120° suggested by the peak in the Al–Cl–Al bond-angle distribution is close to values obtained from *ab initio* MO calculations [7] for $Al_2Cl_7^-$ (125.8°) and similar corner-linked units. However, notwithstanding the apparently high information content of our data, there remains a question as to what information about the 'correct' structure is absent and how this affects the RMC solution. Clearly, it was necessary to try and explore the *range* of possible solution structures especially since isotopic data, and hence a unique set of PSFs, were unavailable.

The first tests conducted were on the effects of varying number density by ±10%. It

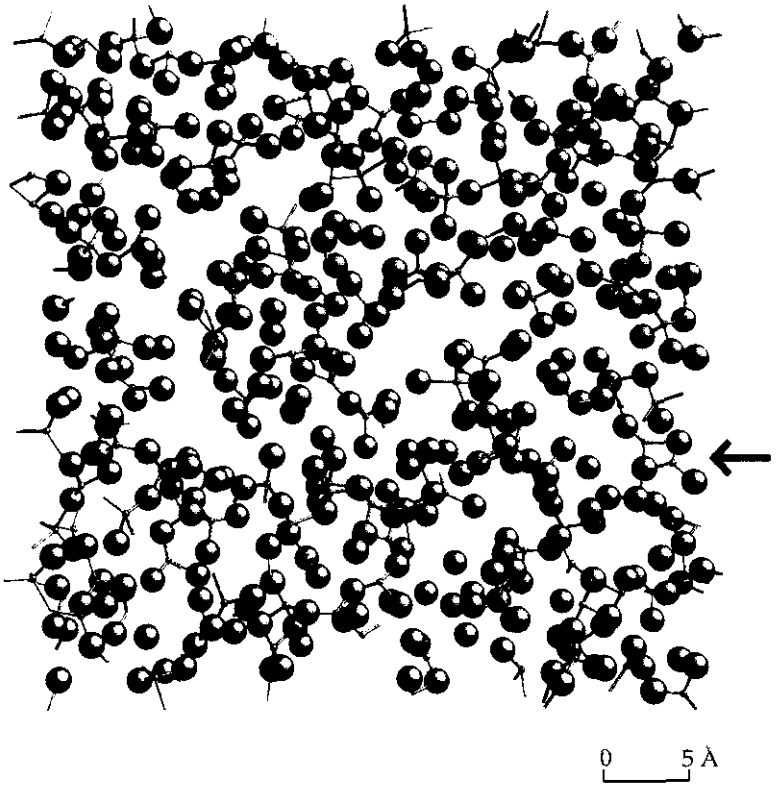

Figure 9. A thick (10 Å) 'slice' through the middle ([200] plane) of a model-I RMC configuration for liquid $AlCl_3$. The 'slice' includes approximately 20% of all the atoms in the simulation cube. The large spheres represent the Cl atoms and the smaller ones the Al; both types have their diameters scaled by 0.5 in order to allow the 'bonds' (a purely geometric definition), between all Al and Cl atoms with separations of less then $r_{max} \sim 2.8$ Å, to be clearly seen. However, this does have the drawback of making it difficult to appreciate the true void volume. The predominance of mainly corner-linked chains is readily apparent although a few instances of edge sharing are visible (a specific example is indicated by the arrow).

was particularly important to check this because of the likely systematic errors in published density measurements due to the difficulties of purifying and handling liquid $AlCl_3$. The main effect of varying the number density was on the vacancies in the local structure of the Al^{3+} ion. For example, reducing the density by 10% generated approximately 10% more vacancies in the local structure and a proportionate reduction in the mean anion coordination number. However, the local geometry of the Al^{3+} ion, as characterized by the relevant bond-angle distributions, was scarcely affected. In addition, bond-network analyses and the Al–Cl–Al and Al–Al–Cl bond-angle distributions indicated that the predominance of chains of mainly corner-linked tetrahedral units was preserved.

However, the critical question to be addressed was whether significant numbers of dimers, or even units possessing the characteristic edge-sharing attribute, were possible in an RMC structure. We attempted to answer this question by reducing the mean Al–Al separation from $\sim$ 3.7 Å, as in model I, to the $\sim$ 3.3 Å expected for dimers, thereby forcing increased edge sharing. This was done by fitting to an artificial $S_{Al-Al}(Q)$ data set

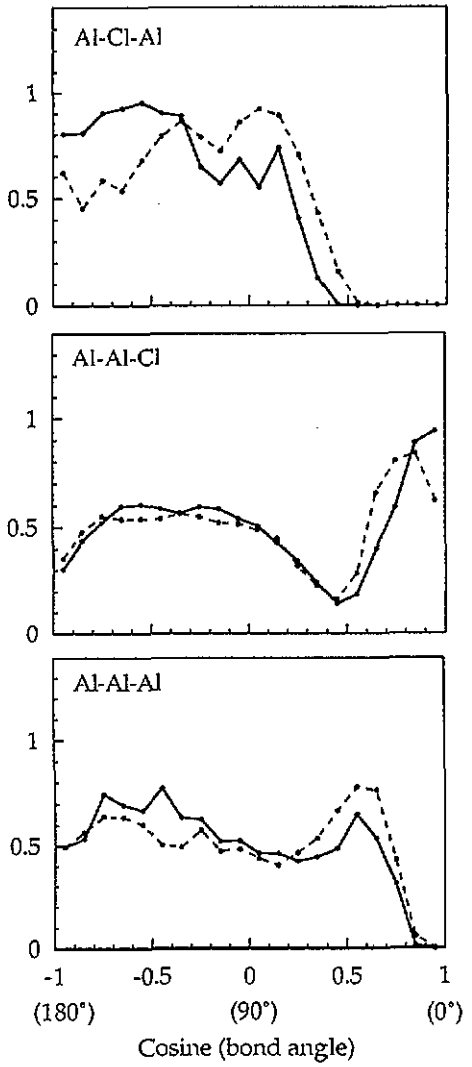

Figure 10. Bond-angle distributions relevant to the wider structure for model I (solid curves) and model II (dashed curves). The Al–Cl–Al function shows the correlations in the bridging angle, viz. the angle formed by atoms 1–8–2 in figure 4. The bridging angle is related by simple geometry to the angle for the Al–Al–Cl function, i.e. the angle formed by atoms 8–1–2 in figure 4.

in addition to the original $F(Q)$. The more direct approach of explicitly including dimers in the initial configuration, and using coordination constraints to preserve these discrete molecules during random moves, had the drawback of requiring a great deal more computer time. The fit to the total structure factor obtained in this case (henceforth referred to as model II) is equally as good as for model I (see figures 5 and 6). Comparison of bond-angle and coordination-number distributions with those of model I (see figures 7 and 8) reveals little change to the local structure. Increased edge sharing is evident from bond-network analysis (table 3) with a larger proportion of connected units containing loops and rings. This appears to be confirmed by the bond-angle distributions (figure 10), with a prominent peak emerging at $\sim 90°$ in the Al–Cl–Al function and with the peak in Al–Al–Cl shifting closer to 45°, just as expected for edge-sharing dimers. However, the Al–Cl–Al function still exhibits a broad peak at $\sim 115°$ and the peak in Al–Al–Cl falls slightly short of 45°. This indicates corner sharing is still a significant feature of the structure. Visual inspection of a series of thin configuration 'slices' (not shown) confirms that although there are at least

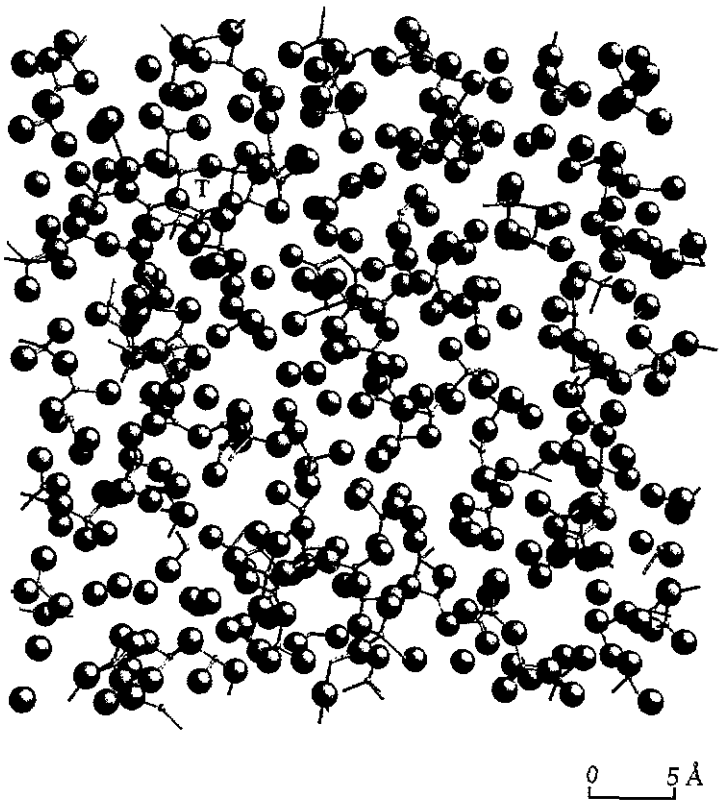

Figure 11. A 'slice' through a model-II RMC configuration corresponding to that for model I in figure 9 (same thickness, plane etc). Although there are now clearly more instances of edge sharing, the overall impression is still of chains of mainly corner-linked, tetrahedral units. What appears to be a 'triplet' of Al atoms (forming part of a larger connected unit) is visible in the top left of the picture and is marked by the symbol 'T' in the middle of the distinctive 'triplet' loop.

50% more instances of edge sharing in the model-II structure compared to model I, chains of mainly corner-linked tetrahedral units still predominate (see figure 11). As regards the possibility of discrete dimers, our RMC results suggest the structure of liquid $AlCl_3$ may be only partially dimerized.

Although the model of liquid $AlCl_3$ as predominantly a fluid of dimers has not been disproved by RMC modelling, it has been shown that an alternative structure consisting mainly of polymeric, mostly corner-linked tetrahedral units is consistent with the data even after allowing for some uncertainty in the $g_{Al-Al}(r)$ partial. If isotopic data were available, the consequent reduction in the range of RMC solutions might make it possible to determine which of the above models is 'correct', particularly if the position of the principal peak in $g_{Al-Al}(r)$ becomes more rigidly constrained†.

† Intriguingly, reducing the Al–Al separation for model II had the effect of greatly increasing the number of rings based on Al 'triplets'. This is shown by the emergence of a peak close to the equilateral 60° angle in the Al–Al–Al bond-angle distribution (figure 10) and confirmed by visual inspection (see figure 11). Reduced uncertainty in the $g_{Al-Al}(r)$ principal-peak position would also make it possible to check whether such 'triplets' are a significant feature of the structure.

Having noted earlier the similarities in some properties of molten $AlCl_3$ and $ZnCl_2$, the general structure suggested by RMC may be best described as a 'sparse network liquid'. The authors favour this new model over the established one because of the greater plausibility of the former when considering the indirect evidence. For example, the greater void volume in liquid $AlCl_3$ compared with $AlBr_3$ can be explained more readily if a skeletal network structure is assumed instead of discrete dimers. Furthermore, because corner-linked $Al_2Cl_7^-$ units have been shown to predominate in $AlCl_3$–KCl melts [7], even at compositions close to pure $AlCl_3$ (75%), and because of the suggestions of higher-order species such as $Al_3Cl_{10}^-$ at the $AlCl_3$-rich end, a distribution of corner-linked tetrahedral polymers in the pure molten salt appears eminently plausible. It should also be pointed out that the low viscosity and conductivity of liquid $AlCl_3$ does not necessarily support the existence of discrete molecules; a 'sparse network liquid', containing voids and large polymeric units of low ionic mobility, would also be consistent with these observations. For the above reasons, the 'sparse network liquid' model of $AlCl_3$ is preferred in the remainder of the discussion on molten salt mixtures and is wholly consistent with the findings.

Table 4. Structural parameters for the Al–Cl principal peak in real space. The peak positions and FWHM values were taken directly from the $G(r)$ functions. The peak height (in $4\pi\rho_0 r^2 g_{Al-Cl}(r)$) for the NaCl mixtures was obtained using the $g_{Al-Cl}(r)$ partial estimated by assuming, at least up to the principal-peak position, an approximately nil contribution to the total $G(r)$ from the other partials.

	Peak position (Å)	Peak height (Å^{-1})	FWHM
$AlCl_3$	2.11 ± 0.02	12.5 ± 1.4	0.37 ± 0.04
% NaCl			
30	2.12 ± 0.02	16.3 ± 1.4	0.35 ± 0.04
45	2.11 ± 0.02	19.1 ± 1.0	0.28 ± 0.04
70	2.11 ± 0.02	18.5 ± 2.0	0.34 ± 0.04
% LiCl			
25	2.11 ± 0.02		
50	2.14 ± 0.02		
70	2.15 ± 0.03		

4.2. Structural modification in the mixtures

The total structure factors and corresponding total pair distribution functions for the molten salt mixtures are shown in figures 12–15. It is apparent from the real-space data that the already well defined local coordination of the Al^{3+} ion becomes better ordered upon the addition of alkali halide while retaining its tetrahedral geometry. Table 4 reveals how the normalized height of the Al–Cl principal peak, estimated from the first peak in $G(r)$, for the $AlCl_3$–NaCl mixtures increases with alkali halide concentration up to at least 45% NaCl. There is also a corresponding reduction in the FWHM despite an increasing contribution on the high-r side from the $g_{Na-Cl}(r)$ partial. In the $AlCl_3$–LiCl mixtures, the height of the first peak in $G(r)$ (which also has its main contribution from the Al–Cl partial) diminishes less rapidly with increasing alkali halide than expected from the simple approximately linear effect of reduced concentration on the FZ coefficient. For example, the peak height in 50% LiCl is clearly more than half the size of that in pure $AlCl_3$, and the peak is unusually sharp. This is all the more remarkable considering the expected negative contribution from the overlapping Li–Cl partial (assuming the principal-peak position remains the same as in pure LiCl). The overlap with the $g_{M-Cl}(r)$ (M = Li, Na) principal peak makes it difficult to

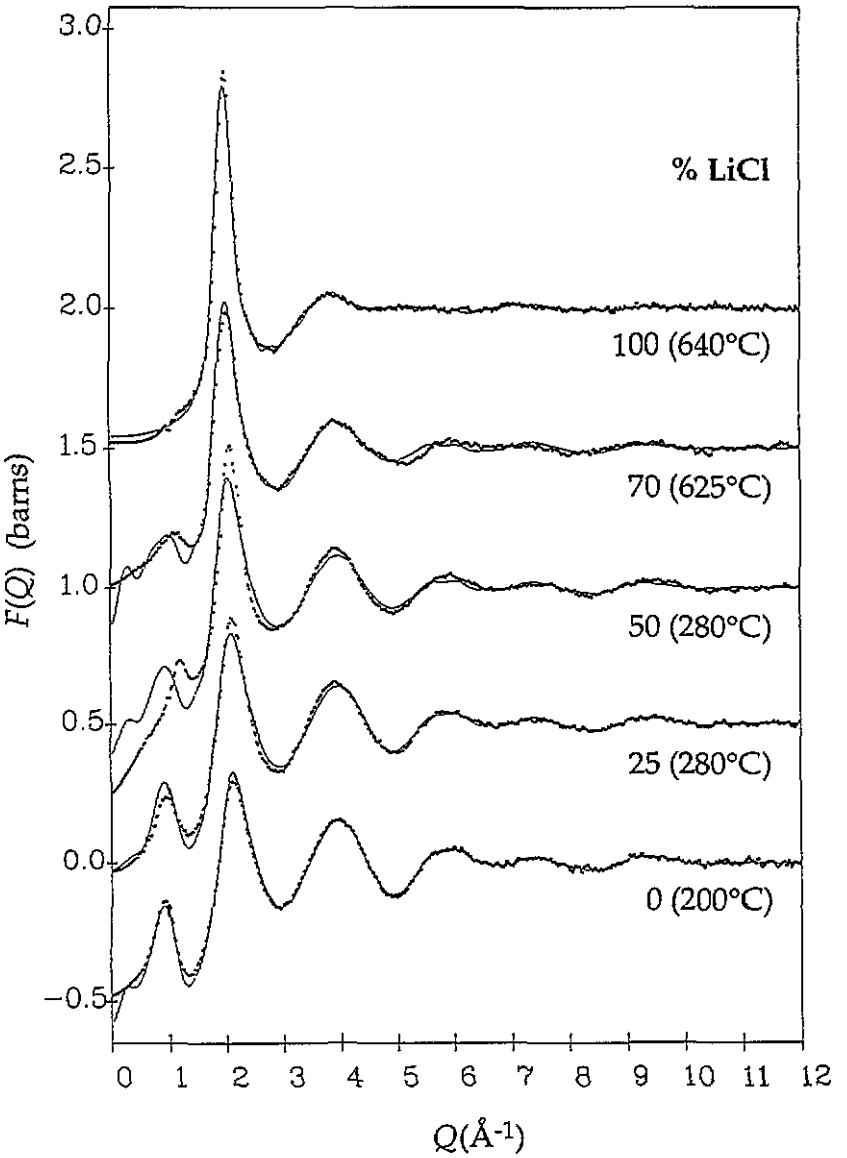

Figure 12. Total structure factor data (dotted curves) for the $AlCl_3$–LiCl molten salt mixtures compared with model functions (solid curves) generated using the pure-salt partials. The partials for pure $AlCl_3$ were from the RMC model-I fit to a single structure factor whereas the partials for pure LiCl were from an RMC fit to isotopic data [28]. Note that in order to maximize use of space, the curves in this figure are in a different sequence to those in the following figures (*13–15*).

reliably estimate the anion coordination from the Al–Cl peak so this has not been attempted. However, evidence for a tetrahedral geometry is provided by the main-peak positions which remain generally unchanged. In the $AlCl_3$–NaCl mixtures, the Al–Cl principal peak remains at a position characteristic of pure $AlCl_3$ (~ 2.11 Å) across the composition range, as does the Cl–Cl peak (~ 3.5 Å), implying no change in the approximately tetrahedral r_{--}/r_{+-} ratio. For the $AlCl_3$–LiCl mixtures, it is harder to draw a similar conclusion because of the

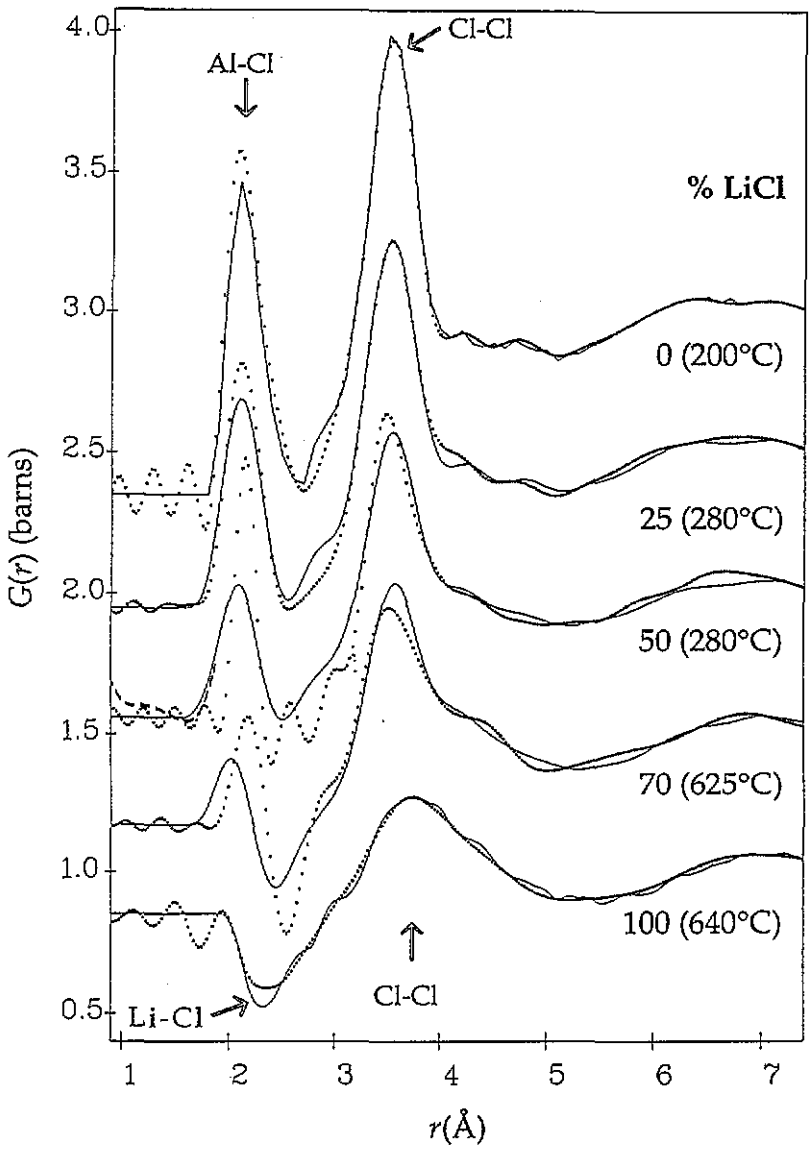

Figure 13. Total pair distribution functions (dotted curves) for the $AlCl_3$–LiCl molten salt mixtures. The FTs of the model structure factors in figure 12 are shown (solid curves) for comparison. The partial structures giving rise to the main peaks in the pure salts are also indicated. In the case of 50% LiCl, the low-r portion of the FT of $F(Q)$ prior to correction for spurious slopes is shown as a dashed line. The absence of a clear peak or trough at $r \sim 1.6$ Å confirms that container subtraction was performed correctly.

proximity of other peaks but the Al–Cl peak position is unaltered at 25% LiCl and the Cl–Cl peak shows no shift even up to 70% alkali halide, suggesting a tetrahedral geometry is also retained in this case. The lack of change in peak positions, especially at the $AlCl_3$-rich concentrations, is wholly consistent with our 'sparse network liquid' model. The Al–Cl principal peak becomes better ordered because of the reduction in longer bridging bonds as

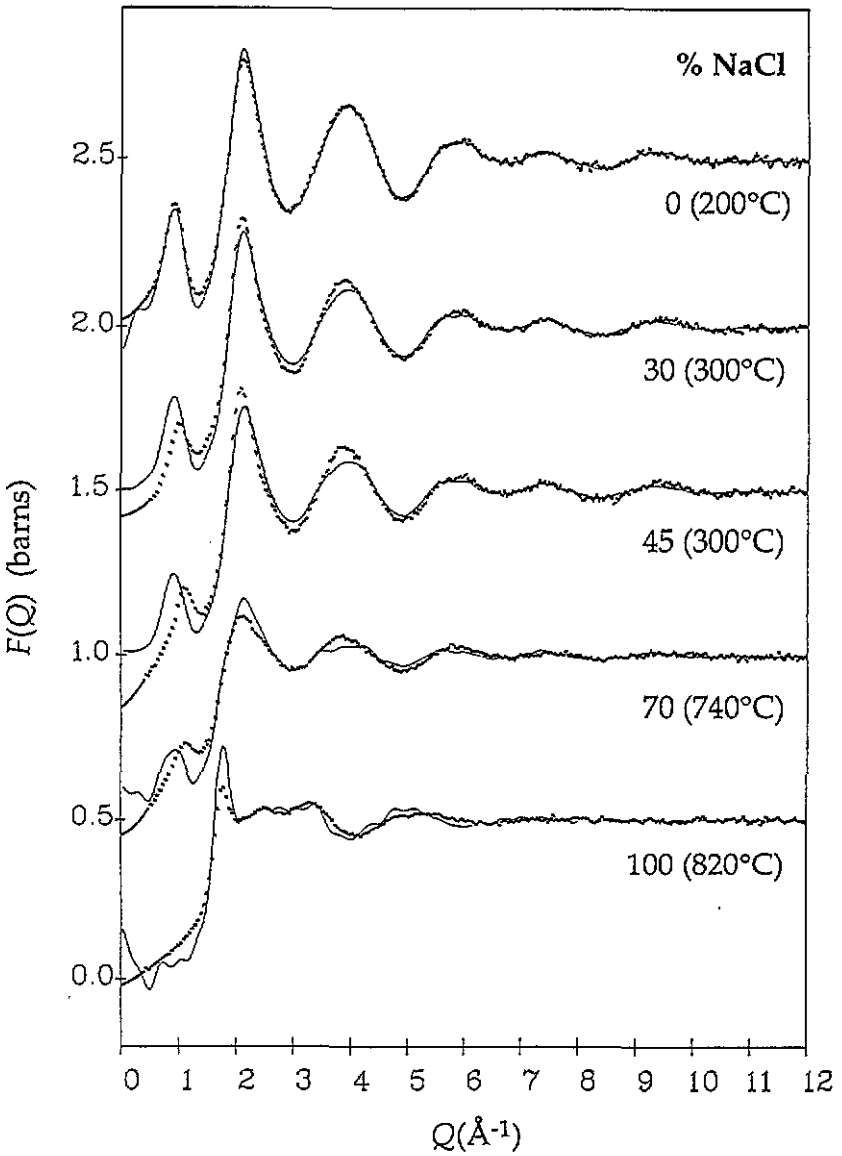

Figure 14. Total structure factor data (dotted curves) for $AlCl_3$–NaCl molten salt mixtures compared with model functions (solid curves) assembled using the pure-salt partials. The partials for pure NaCl are from a RMC fit [29] to the isotopic data of Biggin and Enderby [30]; there is clearly some disagreement with our total structure factor data, particularly in the region of the main peak at $Q \sim 1.8$ Å^{-1}.

large, mainly corner-linked species are broken up.

Modelling studies indicate the Al^{3+} ion dominates the anion structure in the mixtures—this is consistent with the formation of isolated $AlCl_4^-$ units from the breakdown of larger linked species. The data for the mixtures were modelled using the pure-salt partials (those for $AlCl_3$ were from RMC) weighted with FZ coefficients appropriate to each composition. The unavailable M–Al (M = Li, Na) partial could be neglected because of its small weighting.

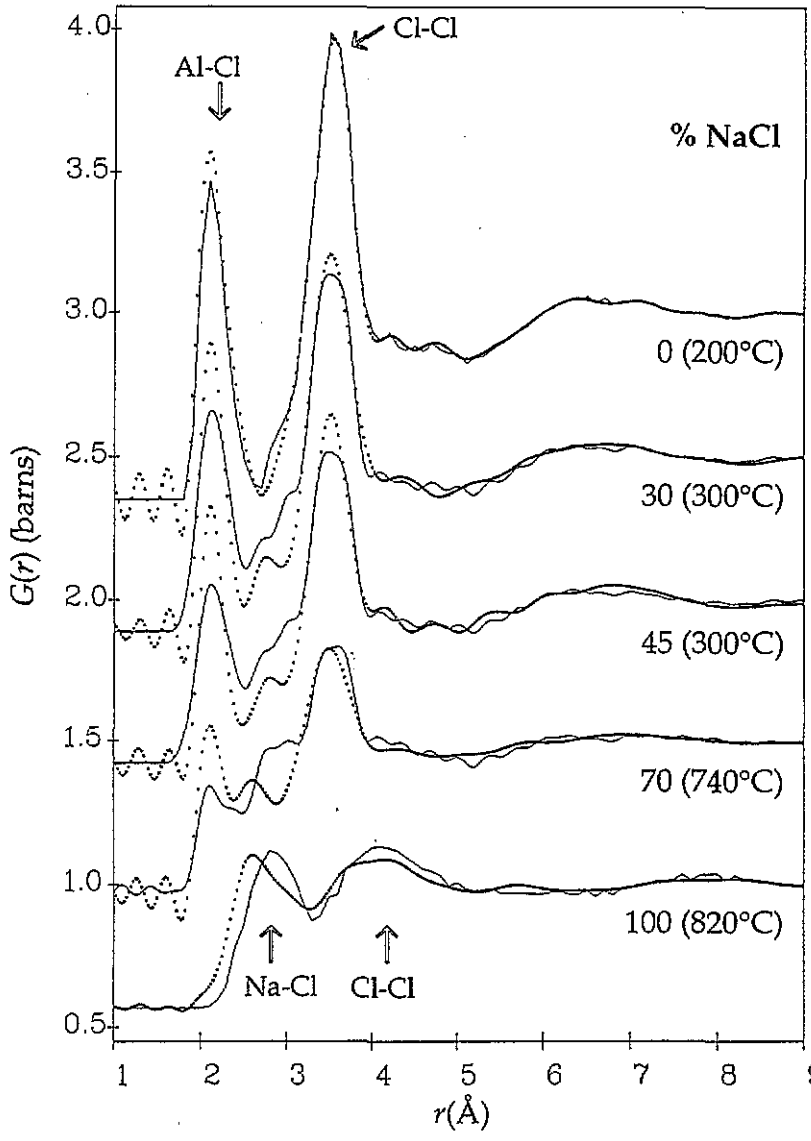

Figure 15. A comparison of actual (dotted curves) and model (solid curves) total pair distribution functions for the $AlCl_3$–NaCl molten salt mixtures. The partial structures giving rise to the main peaks in the pure salts are indicated. The discrepancy between our $F(Q)$ for pure NaCl and that of Biggin and Enderby [30] is apparent in real space mainly as a difference in the Na–Cl principal-peak position. Fortunately, the deviation in the region of the main Cl–Cl peak in the mixtures is small and thus has little effect on modelling of the anion structure.

The distinctive Cl–Cl partial structures for the pure salts, $S^{MCl}_{Cl-Cl}(Q)$ and $S^{AlCl_3}_{Cl-Cl}(Q)$, were both used and their weightings adjusted to obtain the best fit initially to the structure factors. By first working in Q space and only then Fourier transforming using the appropriate number density for the mixtures, it was possible to compensate for the significant effect of density on the partial structures. The FTs of the model structure factors were checked against the

real-space data to confirm an optimum fit in the region of the main anion–anion peaks (see figures 12–15 for a comparison of model fits and data). The resulting best-fit weightings (see table 5) consistently favour the $g^{AlCl_3}_{Cl-Cl}(r)$ partial over $g^{MCl}_{Cl-Cl}(r)$ when compared to the *ideal* weightings expected for simple admixtures of the pure salts. This indicates a dominance of the overall anion structure by the Al^{3+} ion and implies the formation of isolated tetrahedral units from the breakup of larger linked units. However, the best-fit weightings for compositions close to equimolar (50% LiCl and 45% NaCl) do not indicate a complete breakdown, i.e. the reaction $AlCl_3 + MCl \rightarrow AlCl_4^- + M^+$, which suggests there is still a distribution of species. In addition, given the uncertainty in the modelling process (for example, due to errors in the partials† and nominal compositions) the best-fit weightings do not suggest a quantitative difference between the molten salt systems. The results are broadly consistent with the findings of earlier x-ray diffraction studies of the equimolar melts [10, 11]. The weightings for 70% alkali halide, however, are not far short (given the likely errors) of those expected from a complete breakdown into isolated $AlCl_4^-$ units. The high temperatures of these mixtures would be expected to promote such a process. Incidentally, modelling using the pure-salt partials also confirms the increased ordering of the Al–Cl principal peak in the mixtures—it is clearly taller than predicted even for the high-temperature 70% alkali halide samples.

Table 5. The best-fit weightings of the Cl–Cl pure-salt partial structures from modelling the data for the mixtures. The *ideal* weightings expected for admixtures of the pure salts are shown in brackets. Some indication of the errors in the weighting coefficients is provided by the sensitivity of the fitting process: typically a variation of approximately ±0.05 in the best-fit weightings gave a 10% larger χ^2 than the minimum.

	% LiCl			% NaCl		
	25	50	70	30	45	70
$S^{AlCl_3}_{Cl-Cl}(Q)$	0.97 (0.9)	0.85 (0.75)	0.7 (0.56)	0.96 (0.88)	0.92 (0.79)	0.7 (0.56)
$S^{MCl}_{Cl-Cl}(Q)$[a]	0.03 (0.1)	0.15 (0.25)	0.3 (0.44)	0.04 (0.12)	0.08 (0.21)	0.3 (0.44)

[a] M denotes an alkali metal (M = Li, Na).

Our diffraction data also confirm the strong charge ordering in these systems, particularly near the equimolar composition. Charge ordering is suggested by the presence of prominent peaks at $r \sim 6.65$, 9.85 and possibly 12.9 Å in 50% LiCl as well as a weaker peak apparent at $r \sim 6.8$ Å in 45% NaCl. These peaks do not appear to correspond to features in the pure molten salts and this is illustrated in figure 16 by the deviations from model $G(r)$ generated using the pure-salt partials. The new peaks are likely to be associated with the formation of isolated $AlCl_4^-$ tetrahedra, and the size and position suggest they arise mainly from Cl–Cl correlations‡ between these units. From modelling of x-ray diffraction data for equimolar $AlCl_3$ + LiCl [10] and $AlCl_3$ + NaCl [11], Takahashi *et al* suggested a charge-ordered structure with average interunit distances of 6.75 and 6.98 Å, respectively, which appear to be consistent with the peaks observed in our data. The units were assumed to

† The partials in the mixtures will not of course be identical to those in the pure salts. However, the significant effect of density has been taken into account and the findings from our best-fit modelling are in general agreement with those of earlier experiments, which suggests the remaining errors are not large.

‡ Support for this suggestion is provided by an isotopic experiment on equimolar $AlCl_3$ + LiCl [31], indicating the main contribution to the high-r peaks is from $g_{Cl-Cl}(r)$ although this study should not be regarded as conclusive [32].

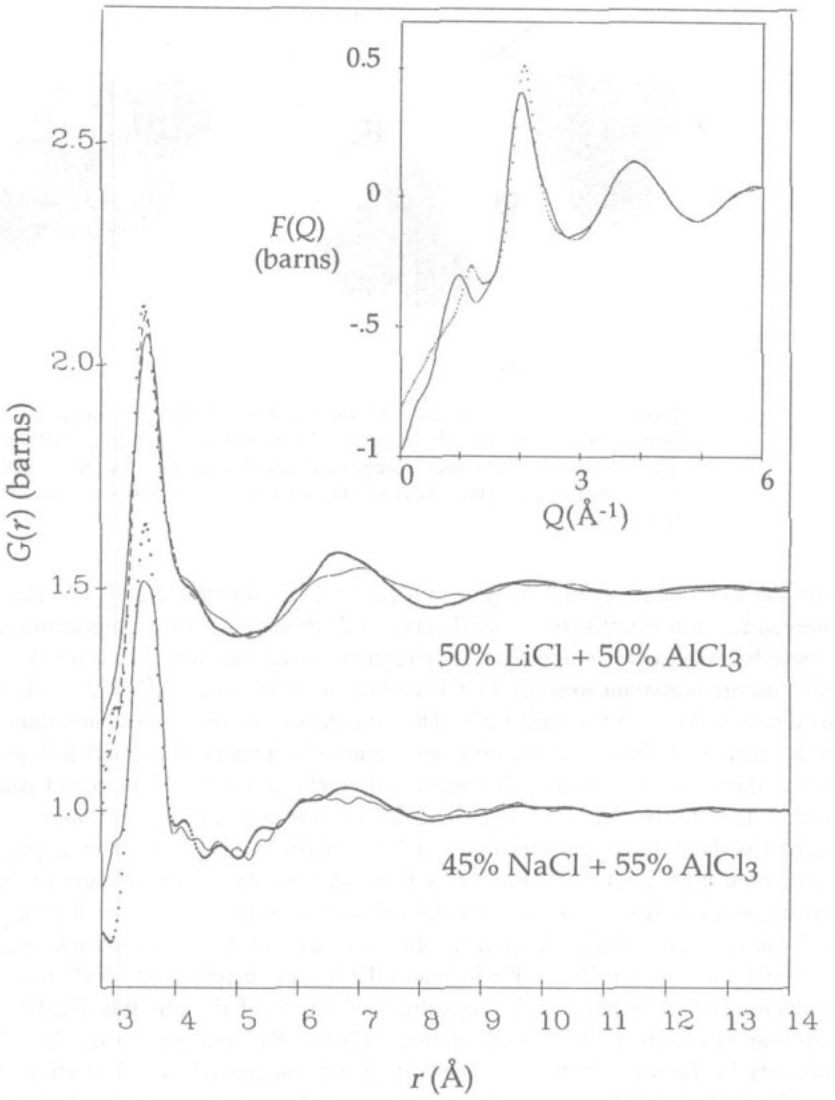

Figure 16. The high-r regions of the $G(r)$ data (dotted curves) for 50% LiCl and 45% NaCl mixtures compared with their respective model fits using the pure-salt partials (solid curves). The maximum-entropy solution for 50% LiCl is also shown (dashed curve) and is almost indistinguishable from the data beyond the main anion–anion peak. The inset compares the original $F(Q)$ for 50% LiCl (dotted curve) with the back transform of the composite $G(r)$ (solid curve) formed by splicing together model ($r \geqslant 5.5$ Å) and data ($r \leqslant 5.5$ Å) real-space functions.

be $MAlCl_4$ (M = Li, Na) hard spheres with the alkali ion located in, or near, face-centre sites of $AlCl_4^-$ tetrahedra. In the case of 50% LiCl, we can extend this model by assuming a close-packed anion coordination around the Al^{3+} ion. Close packing is implied by the RMC coordination-number distribution in figure 8 and is plausible given the small size of the cation. It is now possible to predict the minimum interunit distance as occurring when the faces of neighbouring tetrahedra interlock in a hexagonal close-packed arrangement,

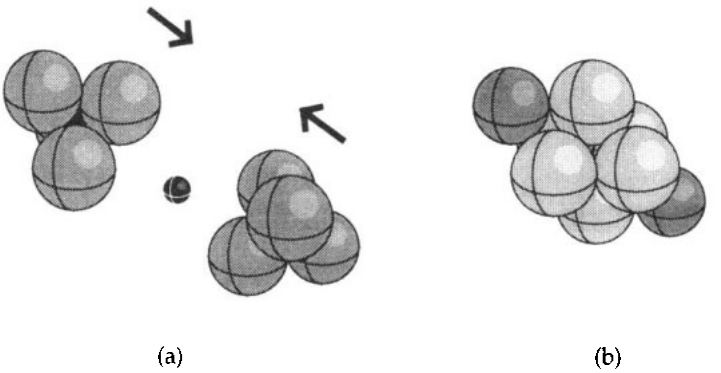

(a) (b)

Figure 17. (a) The 'approach' of two neighbouring $AlCl_4^-$ tetrahedra as a result of charge ordering by the central Li^+ cation and (b) the regular octahedron resulting if the tetrahedra interlock in an AC hexagonal close-packed arrangement (the Cl atoms forming the octahedron have been given a lighter shade of grey for clarity). All atoms are shown approximately to scale.

with the Li^+ ion occupying the gap in the centre, as shown in figure 17. The central singly charged Li^+ ion is unlikely to significantly disturb the faces of neighbouring tetrahedra so it is possible to assume an approximately regular octahedral cage for the alkali cation and thus estimate the *minimum* average Li–Cl separation to be $\sim r_{--}/\sqrt{2} = 2.47$ Å—clearly larger than evident in $G(r)$ for pure LiCl. The divergence between model and data for 50% LiCl in the region of the first minimum (see figure 13) appears to support this simple picture†. Furthermore, the remarkable sharpness and height of the Al–Cl principal peak in $G(r)$, as well as the absence of the expected shift in position to low r (see table 4), is difficult to explain without some movement to higher r of the inverted Li–Cl principal peak from its position in pure LiCl. The picture is less clear for 45% NaCl (primarily because of the inconsistency between our TOF results and earlier isotopic data) but the larger size of the Na^+ ion suggests close packing of tetrahedra would not be possible in this case. Comparison of model and data for 45% NaCl indicates the local structure of the Na^+ ion remains at least as disordered as in pure NaCl, regardless of which of the possible Na–Cl principal-peak positions is assumed. This is consistent with the Na^+ ion occupying disordered sites not precisely in the face centres of tetrahedra, just as suggested by Takahashi *et al* [11].

The question arises as to which features of the structure factor data correspond to the prominent peaks at high r in real space. In order to answer this question the effects in Q space of removing the high-r peaks were estimated for 50% LiCl by splicing together the data ($r \leqslant 5.5$ Å) and model ($r \geqslant 5.5$ Å) $G(r)$ functions and then back transforming (see the inset of figure 16). One effect is to produce a lower, broader peak at $Q \sim 2.0$ Å^{-1} just as expected from the period of ~ 3.1 Å of the observed r-space peaks. Thus the increase in height and narrowing of the main peak at $Q \sim 2$ Å^{-1} noted in both sets of mixtures near the equimolar composition appears to be a consequence, and possibly a characteristic signature, of the strong charge ordering in these systems. The other main effect is a deviation at low Q indicating the additional presence of shallow oscillations of period ~ 5.0 Å in the original $G(r)$, giving rise to the particularly narrow first sharp diffraction peak (FSDP) at

† Possible oversubtraction of container scattering was discounted as a cause of the divergence because tests showed the effect of this to be more closely localized around 2.6 Å than is evident (the difference between model and data extends over the range $r \sim 2.4$–3.0 Å).

$Q \sim 1.2$ Å^{-1} in the unmodified structure factor. The charge-ordered model as discussed above has obvious implications for the intermediate-range structure to which we shall now turn our attention.

4.3. Intermediate-range order

The predominant contribution to the FSDP in the total structure factor for liquid $AlCl_3$ is from $S_{Al-Cl}(Q)$ and not $S_{Cl-Cl}(Q)$. This is evident from the approximately 40% greater height of the FSDP in the x-ray diffraction data [13] compared to our neutron data. The difference is not far short of the $\sim +60\%$ expected from the change in fractional FZ coefficient for $S_{Al-Cl}(Q)$, assuming no contribution from $S_{Cl-Cl}(Q)$ or $S_{Al-Al}(Q)$. Clearly, there is a large FSDP in the $S_{Al-Cl}(Q)$ partial, which has an estimated (absolute) height of ~ 3.5—much greater than in $S^{ZnCl_2}_{Zn-Cl}(Q)$ [22]. There is also a prominent FSDP in $S^{RMC}_{Al-Al}(Q)$, which, because the partial has a very small FZ coefficient, must be essential to fulfilling the additional physical constraints imposed by RMC. The height of the feature is lower than in $S^{ZnCl_2}_{Zn-Zn}(Q)$ [22] but is probably underestimated by the RMC method.

Table 6. The systematic shift in position of the FSDP.

% LiCl	FSDP position (Å)	% NaCl	FSDP position (Å)
25	0.94 ± 0.03	30	1.01 ± 0.02
50	1.18 ± 0.02	45	1.10 ± 0.03
70	1.08 ± 0.02	70	1.12 ± 0.04
$AlCl_3$	0.92 ± 0.02		

A gradual shift in position of the FSDP to higher Q, and a narrowing, is observed up to approximately 50% alkali halide, which implies a systematic reduction in the length scale of intermediate-range order (IRO) in the mixtures. The shift appears to be associated with the formation of a charge-ordered structure because the movement of the FSDP seems to reach its maximum near the equimolar composition (see table 6). A subsequent shift back to lower Q with increased alkali halide, apparent in 70% LiCl at least, can be explained by the increase in temperature and the effects of thermal expansion on the charge-ordered structure. The notable sharpness of the FSDPs at 50% LiCl and 45% NaCl is also consistent with a strongly charge-ordered structure because it suggests IRO extends over many repetition lengths. Despite the expected increase in the average Al–Al separation for such a structure compared to the mainly corner-linked model for pure $AlCl_3$, a reduction in the length scale of IRO in the mixtures is plausible given the possibility of improved packing of tetrahedral units. The packing fractions are close to 50% for both the 50% LiCl and 45% NaCl mixtures, compared to $\sim$ 40% for pure $AlCl_3$. The charge-ordered model also implies an obvious correlation between the maximum FSDP shift and alkali cation size—the smaller Li^+ ion may be expected to force a lower average interunit distance between neighbouring tetrahedra and thus IRO on a shorter length scale, compared to the Na^+ ion. However, although the FSDP position in 45% NaCl is at lower Q than in 50% LiCl, this is not conclusive evidence of such a correlation. The comparison needs to be made at exactly the same equimolar concentration because of the strong compositional dependence of charge ordering in these systems.

It is useful to compare these chloroaluminate melts with other systems in which charge ordering also appears to be linked to IRO, such as molten $NiCl_2$–KCl near the $\frac{2}{3}$ alkali halide concentration [2, 3]. Although little or no shift in FSDP position was observed between pure

$NiCl_2$ and 60% KCl + $NiCl_2$, given the large size of the K^+ ion and the high temperature of the samples (640 °C), this would still appear to be consistent with the suggested correlation between FSDP position and alkali cation size in the mixtures. The isotopic study of equimolar $AlCl_3$ + LiCl by Biggin and co-workers [31] indicated that $S_{Al-Cl}(Q)$ makes the main contribution to the FSDP in the total scattering, which is also likely to be true of 45% NaCl because of the similar size and shape of the feature to that in 50% LiCl. The metal–Cl partial, $S_{Ni-Cl}(Q)$, in 60% KCl + $NiCl_2$ also makes the main contribution to the FSDP in the total scattering, which remains as prominent as in pure $NiCl_2$. In contrast, the clearly diminished size, compared to pure $AlCl_3$, of the FSDP in the 50% LiCl and 45% NaCl mixtures suggests little enhancement of the feature in $S_{Al-Cl}(Q)$ and is consistent with there already being strong IRO in the pure salt.

5. Concluding remarks

From our neutron diffraction data for liquid $AlCl_3$ we have been able to confirm the well defined tetrahedral coordination of the Al^{3+} ion. However, analysis of the total pair distribution function and a review of the historical arguments casts doubt on the established view of the liquid as consisting almost entirely of Al_2Cl_6 dimers. Instead, RMC modelling suggests a 'sparse network liquid' structure which gives both a quantitative fit to the data and is physically consistent. Consideration of the indirect evidence, in particular the much greater void volume in liquid $AlCl_3$ compared to $AlBr_3$, leads the authors to favour the new model over the established one. The 'sparse network liquid' model appears even more plausible given the similarities in some of the physical properties of $AlCl_3$ and $ZnCl_2$. Our proposed structure for liquid $AlCl_3$ can be regarded as the equivalent of the $ZnCl_2$ 'network liquid' only with much reduced connectivity (a 3:1 salt requires less anion sharing, compared with a 2:1 salt, to achieve fourfold coordination). The reduced connectivity and the strong covalent character of bonding readily suggests a sparse network structure with substantial void volume. The authors intend to conduct a detailed isotopic substitution experiment, or possibly a combination of x-ray diffraction and EXAFS measurements, on liquid $AlCl_3$, which should lead to less ambiguous RMC structures. The reduction in the range of feasible structural solutions may make it possible to eliminate one or other of the two basic models discussed. However, it must be acknowledged that obtaining reliable additional structural information, particularly about the all-important Al–Al partial structure, will pose a considerable experimental challenge.

Compared with the divalent metal chloride–alkali chloride mixtures, the main effect of having a smaller, trivalent metal cation in $AlCl_3$–MCl (M = Li, Na) melts appears to be to greatly weaken the dependence of structural modification on alkali cation type. With either type of alkali, the already well defined local coordination of the Al^{3+} ion becomes even better ordered in the mixtures and retains its tetrahedral geometry. In addition, modelling using the pure-salt partials indicates the Al^{3+} ion dominates the anion structure (hence confirming the formation of isolated $AlCl_4^-$ units from the breakdown of larger linked species) with no clear quantitative difference with alkali cation type being discerned. Our diffraction data also confirms the strong charge ordering, particularly near the equimolar composition. A gradual shift in the position of the FSDP to higher Q, and a narrowing, is observed upon the addition of alkali halide up to the 50% concentration. This shift, implying a systematic reduction in the length scale of IRO, appears to be associated with the formation of a charge-ordered structure.

The above findings can be accommodated within the same simple model†, involving competition between two types of cation for anions and hence influence over their respective local structures, as used to explain structural modification in divalent metal chloride–alkali chloride mixtures [2, 3]. In competition against the highly polarizing, triply charged Al^{3+} cation, even the small Li^+ ion can only exert limited influence on the Cl^- ions and hence on the overall anion structure. Our simple model does, however, imply that the highest degree of charge ordering between well ordered $AlCl_4^-$ tetrahedra and alkali counter-ions would occur with the more strongly polarizing Li^+ ion. Because of the strong compositional dependences exhibited by the chloroaluminate systems it has not been possible to confirm this hypothesis in the present study. However, preparations are under way to conduct neutron scattering measurements on a series of equimolar $AlCl_3$ + MCl (M = Li, Na, K, Cs) melts which will allow a systematic comparison of the shape and position of the FSDP. It is also our intention to undertake a detailed isotopic substitution experiment on a specific equimolar melt, probably $AlCl_3$ + LiCl, to obtain PSF information that should make it possible to generate, using RMC, more realistic structures for these highly ordered systems. Again, it must be acknowledged that as with the proposed further study of molten $AlCl_3$, this will be a challenging experiment.

Acknowledgments

We would like to thank the staff at the Rutherford ISIS facility, particularly A K Soper, W S Howells and J Dreyer for their assistance in data collection and analysis. We are indebted to R L McGreevy and J D Wicks for supplying the RMC software and providing much advice about its use. Thanks are also due to M Blander, S J Gurman and S Baker for informal discussions. As always, we gratefully acknowledge the continued support given to this work by the Science and Engineering Research Council and in particular Y S Badyal would like to thank the SERC for awarding him a studentship.

References

[1] Allen D A, Howe R A, Wood N D and Howells W S 1992 *J. Phys.: Condens. Matter* 4 1407–18
[2] Badyal Y S and Howe R A 1993 *J. Phys.: Condens. Matter* 5 7189–202
[3] Badyal Y S and Howe R A 1994 in preparation
[4] Torsi G, Mamantov G and Begun G M 1970 *Inorg. Nucl. Chem. Lett.* 6 553–60
[5] Boxall L G, Jones H L and Osteryoung R A 1973 *J. Electrochem. Soc.* **120** 223–31
[6] Takahashi S, Maruoka K, Koura N and Ohno H 1986 *J. Chem. Phys.* **84** 408–15
[7] Blander M, Bierwagen E, Calkins K G, Curtiss L A, Price D L and Saboungi M-L 1992 *J. Chem. Phys.* **97** 2733–41
[8] Curtiss L A 1987 *Proc. Joint Int. Symp. on Molten Salts* vol 87 (Electrochemical Society) pp 185–94
[9] Rytter E, Rytter B E D, Øye H A and Krogh-Moe J 1973 *Acta. Crystallogr.* B **29** 1541–3
[10] Takahashi S, Muneta T, Koura N and Ohno H 1985 *J. Chem. Soc. Faraday. Trans. II* **81** 319–26
[11] Takahashi S, Muneta T, Koura N and Ohno H 1985 *J. Chem. Soc. Faraday. Trans. II* **81** 1107–115
[12] Semenenko K N and Naamova T N 1964 *Russ. J. Inorg. Chem.* **9** 718–22
[13] Harris R L, Wood R E and Ritter H L 1951 *J. Am. Chem. Soc.* **73** 3151–5
[14] Faber T E and Ziman J M 1965 *Phil. Mag.* **11** 153
[15] Soper A K, Howells W S and Hannon A C 1989 *RAL Report* RAL-89-046
[16] Badyal Y S 1994 *PhD Thesis* University of Leicester, ch 4

† It should be noted that the actual behaviour is certainly more complex than suggested by a simple physical model able to qualitatively explain the facts.

[17] Soper A K 1992 private communication
[18] Sears V F 1992 *Neutron News* **3** 26–37
[19] King L A and Seegmiller D W 1971 *J. Chem. Eng. Data* **16** 23–6
[20] Carpio R A, King L A and Fannin A A Jr 1979 *J. Chem. Eng. Data* **24** 22–4
[21] Boston C R 1966 *J. Chem. Eng. Data* **11** 262–3
[22] Biggin S and Enderby J E 1981 *J. Phys. C: Solid State Phys.* **14** 3129
[23] Palmer K J and Elliott N 1938 *J. Am. Chem. Soc.* **60** 1852–7
[24] Alvarenga A D, Saboungi M L, Curtiss L A, Grimsditch M and McNeil L E 1994 *Mol. Phys.* **81** 409–20
[25] Takahashi S, Koura N, Murase M and Ohno H 1986 *J. Chem. Soc. Faraday. Trans.* II **82** 49–60
[26] Saboungi M-L, Howe M A and Price D L 1993 *Mol. Phys.* **79** 847–58
[27] McGreevy R L and Howe M A 1992 *Ann. Rev. Mater. Sci.* **22** 217–42
[28] McGreevy R L and Howe M A 1989 *J. Phys.: Condens. Matter* **1** 9957
[29] McGreevy R L and Puztai L 1990 *Proc. R. Soc.* A **430** 241–61
[30] Biggin S and Enderby J E 1982 *J. Phys. C: Solid State Phys.* **15** L305
[31] Biggin S, Cummings S, Enderby J E and Blander M 1985 *Proc. 5th Int. Symp. on Molten Salts* vol 86 (Electrochemical Society) pp 81–96
[32] Blander M 1993 private communication